Angular asymmetry and attosecond time delay from the giant plasmon resonance in C_{60} photoionization

T. Barillot, C. Cauchy, P.-A. Hervieux, M. Gisselbrecht, S. E. Canton, P. Johnsson, J. Laksman, E. P. Mansson, J. M. Dahlström, M. Magrakvelidze, G. Dixit, M. E. Madjet, H. S. Chakraborty, E. Suraud, P. M. Dinh, P. Wopperer, K. Hansen, V. Loriot, C. Bordas, S. Sorensen, and F. Lépine

Angular asymmetry and attosecond time delay in tandem from giant plasmon in C_{60} photoionization

T. Barillot[1], C. Cauchy[1], P-A. Hervieux[2], M. Gisselbrecht[3], S. E. Canton[4], P. Johnsson[3], J. Laksman[3], E. P. Mansson[3], J. M. Dahlström[5], M. Magrakvelidze[6], G. Dixit[7], M. E. Madjet[8], H. S. Chakraborty[6], E. Suraud[9], P.M. Dinh[9], P. Wopperer[9], K. Hansen[10], V. Loriot[1], C. Bordas[1], S. Sorensen[3] and F. Lépine[1]

[1]*Institut Lumière Matière, UMR5306, Université Lyon 1-CNRS,*
10 rue Ada Byron, 69622 Villeurbanne cedex, France
[2]*Institut de Physique et Chimie des Matériaux de Strasbourg,*
23 rue du Loess, BP 43, 67034 Strasbourg Cedex 2, France.
[3]*Department of Physics, Lund University, Box 118, 221 00 Lund, Sweden*
[4]*Department of Synchrotron Radiation Instrumentation,*
Lund University, Box 118, 221 00 Lund, Sweden
[5]*Department of Physics, Stockholm University, Alba Nova University Centrum, S-106 91, Stockholm, Sweden*
[6]*Department of Natural Sciences, Center for Innovation and Entrepreneurship,*
Northwest Missouri State University, Maryville, Missouri 64468, USA
[7]*Max Born Institute, Max-Born-Strasse 2A, 12489 Berlin, Germany*
[8]*Qatar Energy and Environment Research Institute (QEERI), P.O. Box 5825, Doha, Qatar*
[9]*Laboratoire de Physique Théorique, IRSAMC, Université de Toulouse,*
UPS, F-31062 , France and CNRS, F-31062 Toulouse, France. and
[10]*Department of Physics University of Gothenburg SE-41296 Gothenburg, Sweden*

This combined experiment-theory study demonstrates that the surface plasmon resonance in C_{60} alters the valence photoemission quantum phase, resulting in strong effects in the photoelectron angular distribution and emission time delay. Electron momentum imaging spectroscopy is used to measure the photoelectron angular distribution asymmetry parameter that agrees well with our calculations from the time-dependent local density approximation (TDLDA). Significant structure in the valence photoemission time delay is simultaneously calculated by TDLDA over the plasmon active energies. Results reveal a unified spatial and temporal asymmetry pattern driven by the plasmon resonance, and offers a sensitive probe of electron correlation. A semiclassical approach facilitates further insights into this link that can be generalized and applied to other molecular systems and nanometer-sized metallic materials exhibiting plasmon resonances.

I. INTRODUCTION

The study of the collective excitation of electrons, or plasmons, in nano-size systems is a subject of broad interest. For clusters and nanostructures, plasmons have direct consequences for the optical properties of the material, e.g., photoabsorption and photoemission. As the characteristics of the plasmon can be controlled by changing the size and geometry of the system, understanding the properties of the plasmon offers the possibilities to design nano-systems for use in, for instance, optoelectronic applications. From a fundamental point of view, a plasmon is in itself a "laboratory", which can be used to understand multi-electronic effects in a bosonic system composed of a large number of interacting fermions.

The case of the fullerene molecule, C_{60}, is especially intriguing because a giant surface plasmon resonance has been discovered around 20 eV. It was first predicted by Bertsch and co-workers in 1991 [1] within the framework of the linear-response theory and it was observed experimentally in 1992 [2, 3]. This resonance corresponds to a collective oscillation of delocalized π electrons relative to the ionic cage. The lifetime of the plasmon in C_{60}, estimated from the width of the resonance, is close to one femtosecond, and therefore corresponds to electron dynamics occurring on the attosecond timescale. With recent developments in technology, such ultrafast dynamics have become accessible experimentally [4]. Attosec-

ond science has led to several applications such as the measurements of Auger decay lifetime in atoms [5, 6], charge localization in molecules [7, 8] or time delays in photoemission [9]. These developments call for further investigation in systems of increasing complexity [10]. In connection with fullerenes, theoretical time delays have been simulated, using time-dependent local density approximation (TDLDA), for endohedrally confined argon atom inside C_{60} [11], addressing the role of atom-fullerene hybridization on photoemission time delays.

Giant correlation effects strongly alter the quantum phase associated with the amplitude of the photoemission at plasmon energies. One direct consequence is a change of the asymmetry in photoelectron dipolar angular distribution due to the interference term $\cos(\varphi_{\ell+1} - \varphi_{\ell-1})$, where φ are the quantum phases of two dipole allowed channels from an initial state of ℓ angular momentum. This asymmetry, which depends on the relative phase, $\varphi_{\ell+1} - \varphi_{\ell-1}$, can be thought of as distortions in space-distribution of photoelectrons. In contrast, a second consequence of the plasmon-induced phase variation is the distortion in photoelectron temporal profile characterized by the Wigner time delay [12], the energy derivative of the total phase, $\varphi_{\ell+1} + \varphi_{\ell-1}$, appropriately weighted. Hence, both space-like and time-like distortions are conjoined in birth via the phase and they can provide complementary accesses into the plasmon semiclassical dynamics, providing, in combination, a powerful spectroscopic tool never attempted before. In this ar-

ticle, we present photoionization asymmetry parameter (β) measurements in the vicinity of the surface plasmon resonance of C_{60}; the photoelectron momentum imaging technique was used to characterize the ionization process. Comprehensive calculations using TDLDA, that had good success to describe earlier experiments [3, 13], concur with our measurements and also predict, for the first time, strong variations in the photoemission time delay on the attosecond scale for this resonance. Model calculations within WKB approximation are presented to get a physical insight into the process.

II. EXPERIMENTAL DETAILS

So far, angle-resolved photoelectron spectra of vapor-phase C_{60} were reported for a large photon energy range [14–16]. In those experiments, β was found to vary significantly with the photon energy, but no detailed investigation around the plasmon resonance has been reported. Our experiment was carried out at the I3 beamline of the MAX-Lab synchrotron facility that delivers XUV radiation between 4 and 50 eV. We used a resolution of 0.1 eV for a typical photon flux of 10^{12} photons/s. A molecular beam of pure C_{60} was produced by an oven maintained at a temperature of 800 K while a Velocity Map Imaging Spectrometer (VMIS) [17] was placed perpendicularly to both photon beam and molecular beam. The entire setup was maintained at a pressure of 10^{-9} mbar. The VMIS had a standard design composed of three electrodes creating an inhomogeneous static electric field that accelerated the electrons and focused their trajectories onto a position sensitive detector (PSD). The detector consists of dual microchannel plates followed by a phosphorus screen and imaged by a CCD camera.

III. RESULTS

The plasmon resonance at 20 eV in C_{60} is located well above the ionization threshold at 7.6 eV. In figure 1, we present a typical result. The raw image as well as the angle integrated photoelectron spectrum recorded at 20 eV photon energy are shown. The spectrum reveals peaks at 12.4 eV and 11.1 eV corresponding to ionization from the HOMO (5hu state) and HOMO-1 (4hg and 4gg states) orbitals of C_{60} as identified by Liebsch and co-workers [14]. A third peak is identified at lower kinetic energy ($\sim$ 8.5 eV) and corresponds to transitions from σ-orbitals to the continuum. For lower photoelectron kinetic energy the spectrum corresponds to the combinations of direct and autoionization pathways. This last part of the spectrum has an isotropic angular distribution. On the contrary, the contributions of the HOMO and HOMO-1 orbitals appear as two isolated contributions with an angular distribution which is aligned along the light polarization (vertical in the figure). The measured β is shown as a function of photon energy ranging from 17 to 22 eV (figure 2, blue dots) along with the calculated β (grey curves). The calculation is performed using TDLDA with

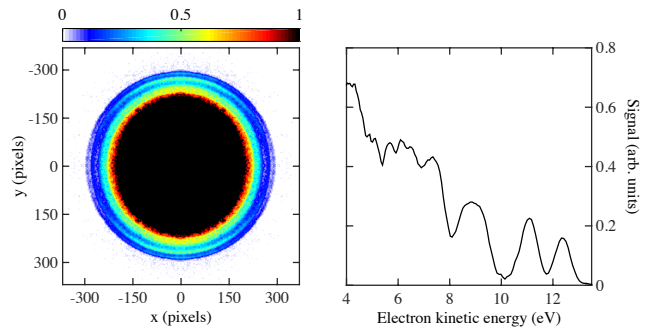a jellium representation of the C_{60} molecule [18].

FIG. 1. (Color online) 2D projection of the photoelectron velocity distribution (left) and corresponding angularly integrated photoelectron kinetic energy spectrum (right) for C_{60} measured at synchrotron photon energy of 20 eV. The two peaks at 12.4 eV and 11.1 eV correspond to ionization from the HOMO and HOMO-1 orbitals, respectively.

TDLDA predict that the β increases smoothly and quasi-linearly with the photon energy when no plasmon resonance is present around 20 eV (grey dashed curve). On the contrary, when the plasmon resonance is included in the calculation in that spectral range by taking into account correlation effects (grey plain curve), a noticeable variation in β is observed within this energy range, which shows that the β is sensitive to the presence of the plasmon resonance. Our calculations are in good agreement with the experimental results, if the effect of the plasmon is taken into account. For both molecular orbitals, a minimum of β is reached near the resonance frequency while it increases for a blue or red shifted wavelength. Let us notice that slightly lower β values were found above 20 eV in [15] using a double time-of-flight technique. In our work, the investigation of the complete photon energy range around the resonance shows clear variations and a minimum in β around the maximum of the resonance. The differences between calculations and experimental data can be explained by the role of temperature of the molecule that would smoothen the PAD in the experiment.

In addition to calculation of the β value, the phases of two dipole channels from each orbital are also used to extract dynamical information, namely, the photoemission Wigner time delay by energy-differentiating the sum of the two phases weighted by the corresponding channel strength. Besides the regular Coulomb and short-range phases from single-electron effects, the TDLDA phase also includes the correlation phase, φ_c, arising from the plasmon. For simple atomic systems, the photoemission time delay has recently become experimentally accessible [9, 19, 20]. In these experiments, phase shifts were measured for the photoemission from two different orbitals using two-color electron interferometric techniques. Such measurement has also been performed on diatomic molecules to study the influence of autoionizing resonance [21, 22]. In our case, we consider the influence of
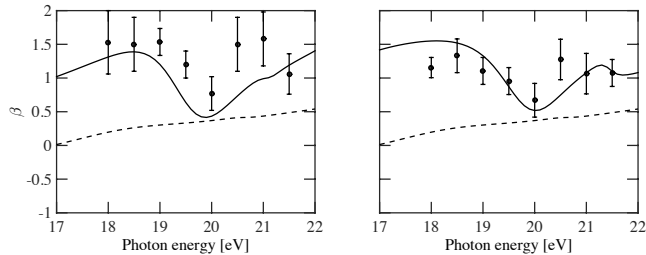
FIG. 2. Experimental and theoretical variation of the asymmetry parameter, β, around the plasmon resonance for HOMO (left) and HOMO-1 (right). Dots: experimental data points. Curves: TDLDA calculation with the inclusion of the plasmon resonance at 20 eV (plain) or without including the plasmon resonance (dashed).

the plasmon on the photoemission time delay when the photon energy is tuned around the resonance by comparing the Wigner delay with and without φ_c. More specifically, we investigate the additional time delay induced by the plasmon resonance for photoelectrons emitted from HOMO and HOMO-1 orbitals, which also exhibit strong variations in the β value around the same spectral region. Results are presented in figure 3.
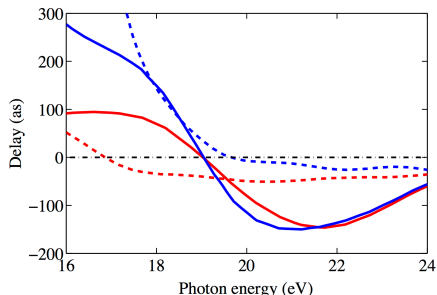

FIG. 3. (Color online) Variation of photoemission time delays for HOMO (red) and HOMO-1 (blue) photoelectrons with photon energy calculated in TDLDA. Corresponding delays without the correlation phase φ_c are shown in dashed curves.

As evident, the photoemission time delay varies non-monotonously for both the orbitals (HOMO and HOMO-1) around the plasmon resonance. At excitation energies lower than the resonance, the photoelectrons are decelerated, but on the contrary appear accelerated above the resonance. At energies higher than 24 eV, the TDLDA delays coincide with the results obtained by excluding φ_c.

IV. DISCUSSION

The link between the sharp variation of the photoelectron angular distribution and the variation of the photoemission time delays of photoelectrons can be understood based on first principle considerations using the following

model. When the C_{60} molecule absorbs an XUV photon, the photoexcitation process is determined by the complex interaction between the 240 valence electrons of the molecule and the incident photon. Without solving the full time-dependent many-body problem, one can mimic the effect of these many body interactions by introducing an effective Hamiltonian as

$$\hat{H}_{eff} = \hat{H}_0 + \hat{H}_p + \hat{V}_L. \tag{1}$$

Note that all the equations presented in this article are expressed in atomic units ($\hbar = m_e = e = 1/4\pi\epsilon_0 = 1$). In a first approximation, we consider the effect of the plasmon resonance on the ionization mechanism by introducing a correction term, $\hat{H}_p$, to the field-free Hamiltonian of the molecule $\hat{H}_0$, and $\hat{V}_L$ represents the interaction Hamiltonian with the incident radiation. $\hat{H}_p$ corresponds to the average effect of the collectively excited electrons and is represented by a dipolar screening potential V_{scr} [18] and written as

$$V_{scr}(\vec{r}, \omega) = V_{scr,r}(r, \omega)\cos(\theta). \tag{2}$$

Here, $V_{scr,r}$ is the radial part of the screening potential defined classically for C_{60} in [23], r is the distance from the center of the molecule, ω is the incident photon energy and θ is the angle with respect to the light polarization. We consider the effect of the screening potential on the radial part of the continuum wave function $\psi_\epsilon(r, \theta, \varphi)$ only, where ϵ is the electron kinetic energy. Assuming the usual separation of variables for a spherical potential, the continuum wavefunction can be written as $\psi_{\epsilon, \ell\pm1, m}(r, \theta, \varphi) = \frac{P_{\epsilon, \ell\pm1}(r)}{r} Y_{\ell\pm1, m}(\theta, \varphi)$, m is the magnetic momentum of the initial state. $Y_{\ell\pm1, m}(\theta, \varphi)$ is the spherical harmonic and the radial part $P_{\epsilon, \ell\pm1}(r)$ of the wavefunction is found by using the semiclassical WKB approximation in one dimension [24, 25]. This framework has the advantage to express the potentials that photoelectrons experience as phase terms $\Delta_{\ell\pm1}(\epsilon, r)$ of the wavefunction of the form $P_{\epsilon, \ell\pm1}(r, \omega) \propto \sin(kr + \Delta_{\ell\pm1}(\epsilon, r))$; Δ sums up the Coulomb and short-range phase. Therefore, the plasmon potential invokes an additional phase (which is the analogue of TDLDA correlation phase φ_c):

$$\phi(\epsilon, \omega) \approx -\int_{r_c}^{\infty} \frac{\Re e[V_{scr,r}(r, \omega)]}{\sqrt{2\epsilon}} dr. \tag{3}$$

Here, $\phi(\epsilon, \omega)$ is a parameterized function of ω as the screening potential depends on ω, r_c is the classical turning point and is different for $\ell+1$ and $\ell-1$ partial waves but this difference induces a negligible variation. This additional phase term has a direct influence on the transition probability between the initial bound wavefunction and final continuum partial waves through the reduced transition dipole moment:

$$d_{\ell\pm1} = \sqrt{(2l+1)(2(l\pm1)+1)} \begin{pmatrix} \ell & 1 & \ell\pm1 \\ 0 & 0 & 0 \end{pmatrix} \\ \times \int P_{\epsilon, \ell\pm1}(r) V_L(r) P_{n, \ell}(r) dr \tag{4}$$

where the expression of the initial wavefunction $P_{n, \ell}(r)$ (where n is the principal quantum number) is based

on DFT (Density Functional Theory) ground state calculation of C_{60} by M.E. Madjet & al. [13].

The asymmetry parameter β can be derived directly from the transition dipole moments in spherical coordinates. Note that this parameter is sometimes introduced as a function of the radial transition dipole element [26, 27]. Following reference [18], we used a formulation that depends on the reduced dipole element. We recall here this expression for a particular sub-shell n, ℓ:

$$\beta_{n,\ell}(\omega) = \frac{\{(\ell+2)|d_{\ell+1}|^2 + (\ell-1)|d_{\ell-1}|^2}{+6\sqrt{\ell(\ell+1)}\Re e[d_{\ell+1}d_{\ell-1}^* e^{i(\Delta_{\ell+1}-\Delta_{\ell-1})}]\}} \times [(2\ell+1)(|d_{\ell+1}|^2 + |d_{\ell-1}|^2)]^{-1} \tag{5}$$

Using the simplified description of the plasmon influence defined above, we can compute the value of β as a function of the photon energy around the resonance. The results of the analytical calculation with the plasmon resonance taken into account are presented in figure 4 by plain red curves for both HOMO and HOMO-1. A clear variation around the plasmon resonance, similar to the one obtained using TDLDA method, is observed indicating that the phase term $\phi(\epsilon, \omega)$ reproduces correctly the effect of the plasmon on the electron continuum wavefunction and thereby on the asymmetry parameter. The differences observed between analytical and TDLDA calculations of β come from the fact that the angular distribution is very sensitive to electron correlation. Therefore, the semiclassical treatment only includes a rough description of the process and only reveals the main trend.
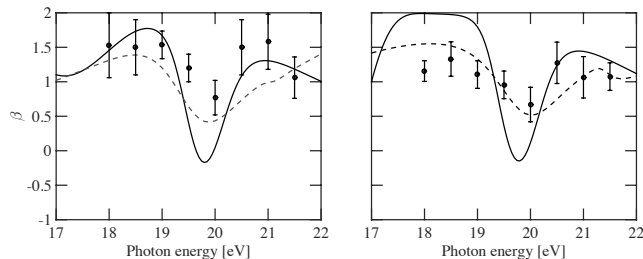
FIG. 4. Comparison between TDLDA and semiclassical calculations of variation of the asymmetry parameter β around the plasmon resonance for HOMO (left) and HOMO-1 (right). Plain curves: semiclassical model calculation. Dashed curves: TDLDA calculation. Dots: experimental data points.

The formulation of the plasmon resonance influence on photoemission as an additional phase term in the continuum wavefunctions allows a direct connection to the dynamics evidenced in TDLDA. Using once again the concept of Wigner time delay, the *extra* delay induced by $V_{scr,r}$ for the electron to escape the potential is expressed as:

$$\tau_W = \frac{\partial \phi(\epsilon, \omega)}{\partial \epsilon}. \tag{6}$$

In figure 5-a, we have calculated the photoemission time delay, τ_W, induced by the plasmon potential. The result of the calculation is shown as a function of the photon energy. It is explained by the variation of the real part of the screening potential, as shown in figure 5-b, which is positive before the maximum, zero at the maximum and negative at higher photon energy. In a classical picture, the ejected electron leaving from the C_{60} shell has a reduced or increased local momentum in the effective molecular potential which is asymptotically encoded in its phase. Therefore, it is expected that the photoemission time varies around the resonance. We also demonstrate with this result that the exact same trend observed in the TDLDA calculation is obtained with our model with slightly lower delays in this case.
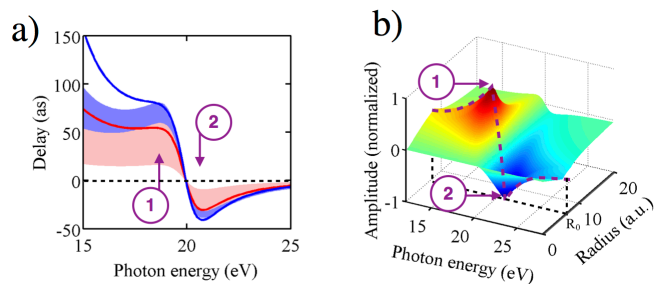
FIG. 5. (Color online) Photoemission time delay variation associated with change in the screening potential. a) Photoemission time delay for HOMO (red curve) and HOMO-1 (blue curve) photoelectrons in the semiclassical model (plain curves). Filled areas correspond to the classical electron photoemission time from HOMO (red area) and HOMO-1(blue area). b) Real part of the potential $V_{scr,r}$ as a function of the photon energy and distance [23]. The purple dashed line represents the C_{60} radius (R_0) and positions 1 and 2 are respectively the maximum and minimum of screening.

In addition, we consider the classical calculation of an electron propagation through the screening potential. The photoemission time variation starting from different initial positions is represented on figure 5-a) by a shaded area (red from HOMO and blue from HOMO-1 orbital). This distribution of time delays is compared to the one that is calculated with the phase shift induced by the same potential on the continuum wavefunction (see equations (3), (6) and solid lines in figure 5-a). The differences observed at low excitation energies come from the perturbative treatment of the plasmon potential in the WKB approach. At higher excitation energy, the higher photoelectron kinetic energy makes this approximation more valid. The fact that the WKB calculation matches the classical estimation corroborates the physical meaning of the Wigner time delay in this particular case. A maximum variation of ~ 50 attoseconds for the HOMO photoelectron has been predicted semiclassically and reaches almost 200 attoseconds in TDLDA. It is especially interesting that this time delay lies in the attosecond domain. Let us mention that the 20 attoseconds time delay in the photoemission from 2s and 2p orbitals of Ne was mea-

sured in reference [9], the same order of magnitude as the ones considered in our investigation and that, consequently, should be experimentally accessible although the complex electronic structure of C_{60} makes the experiment extremely challenging for current experimental possibilities.

The unique complementarity between the photoelectron asymmetry parameter and photoemission time delay can be understood by drawing parallels between the quantum phase and the momentum in the mechanical world [11]. Consider a two-particle system of motion. If their relative momentum alters in time, then there must be an external force acting on the system. Since the external force is the time derivative of the total momentum, the changes in the relative momentum and the application of a force must be simultaneous and correlated. As time and energy are canonical conjugates, the analogue of the force is the Wigner delay, pointing at the fundamental connection between the asymmetry and delay via the phase.

V. CONCLUSION

In conclusion, we report the investigation of the photoelectron angular distribution around the plasmon resonance in C_{60} and its link to photoemisssion time delays, which are on attosecond time scale. We have shown that the plasmon-induced potential re-shapes the angular distribution of photoelectrons around the resonance. This is correlated with a variation of the photoemission time delay on the attosecond timescale. These variations are strongly dependent on the exact treatment of electron correlation. Consequently, the combination of angular distribution and photoemission delay analysis paints a picture of complete space and time asymmetry of emission, and could be used to probe very accurately electron correlation effects in plasmons. The validation of the process with a simple analytical model as well as many-body theory calculations indicates the generality of the effect which is therefore applicable to other large molecular systems or to metallic nano-sized materials exhibiting a plasmon resonance.

[1] G. F. Bertsch, A. Bulgac, D. Tománek, and Y. Wang, Phys. Rev. Lett. **67**, 2690-2693 (1991).
[2] I.V. Hertel, H. Steger, J. de Vries, B. Weisser, C. Menzel, B. Kamke, and W. Kamke, Phys. Rev. Lett. **68**, 784-787 (1992).
[3] S.W.J. Scully *et al.*, Phys. Rev. Lett. **94**, 065503 (2005).
[4] P. Antoine, A. L'Huillier, and M. Lewenstein, Phys. Rev. Lett. **77**, 1234-1237 (1996).
[5] M. Drescher, M. Hentschel, R. Kienberger, M. Uiberacker, V. Yakovlev, A. Scrinzi, Th. Westerwalbesloh, U. Kleineberg, U. Heinzmann and F. Krausz, Nature **419**, 803-807 (2002).
[6] S. Zherebtsov, A. Wirth, T. Uphues, I. Znakovskaya, O. Herrwerth, J. Gagnon, M. Korbman, V.S. Yakovlev, M.J.J. Vrakking, M. Drescher and M.F. Kling, J. Phys. B **44**, 105601 (2011).
[7] G. Sansone *et al.*, Nature **465**, 763 (2010).
[8] Ch. Neidel *et al.*, Phys. Rev. Lett. **111**, 033001 (2013).
[9] M. Schultze *et al.*, Science **328**, 1658 (2010).
[10] F. Lépine, M.Y. Ivanov and M.J.J. Vrakking, Nat. Photonics **8**, 195-204 (2014)
[11] G. Dixit, H.S. Chakraborty and M.E. Madjet, Phys. Rev. Lett. **111**, 203003 (2013)
[12] E.P. Wigner, Phys. Rev. **98**, 145-147 (1955).
[13] M.E. Madjet, H.S. Chakraborty, J.M. Rost and S.T. Manson, J. Phys. B **41**, 105101 (2008).
[14] T. Liebsch, O. Plotzke, F. Heiser, U. Hergenhahn, O. Hemmers, R. Wehlitz, J. Viefhaus, B. Langer, S.B. Whit-field, and U. Becker, Phys. Rev. A **52**, 457-464 (1995).
[15] S. Korica, D. Rolles, A. Reinköster, B. Langer, J. Viefhaus, S. Cvejanovic, and U. Becker, Phys. Rev. A **71**, 013203 (2005).
[16] F.A. Gianturco and R.R. Lucchese, Phys. Rev. A **64**, 032706 (2001).
[17] A.T.J.B. Eppink and D.H. Parker, Rev. Sci. Instrum. **68**, 3477 (1997).
[18] E. Maurat, P.A. Hervieux and F. Lépine, J. Phys. B **42**, 165105 (2009).
[19] D. Guénot *et al.*, Phys. Rev. A **85**, 053424 (2012).
[20] K. Klünder *et al.*, Phys. Rev. Lett. **106**, 143002 (2011).
[21] S. Haessler *et al.*, Phys. Rev. A **80**, 011404 (2009).
[22] J. Caillat, A. Maquet, S. Haessler, B. Fabre, T. Ruchon, P. Salières, Y. Mairesse, and R. Taïeb, Phys. Rev. Lett. **106**, 093002 (2011).
[23] J.U. Andersen and E. Bonderup, Eur. Phys. D **11**, 413 (2000).
[24] H. Friedrich, "Theoretical atomic physics" (Berlin: Springer), (1994)
[25] J M Dahlström, A L'Huillier and A Maquet, J. Phys. B **45**, 183001 (2012).
[26] J. Cooper and R.N. Zare, J. Chem. Phys. **48**, 942?943 (1968).
[27] J. Cooper and R.N. Zare, J. Chem. Phys. **49**, 4252 (1968).